Endocrine Imaging: Parathyroid, Adrenal Cortex and Medulla, and Other Endocrine Tumors. Part II

William H. Beierwaltes

St. John Hospital and Medical Center, Detroit, Michigan

J Nucl Med 1991; 32:1627–1639

PARATHYROID GLAND

Prevalence of Primary Hyperparathyroidism

The most common cause of hypercalcemia in ambulatory patients is primary hyperparathyroidism (HPT). Approximately one in every 1000 adults has the disease. Approximately 1 in every 200 elderly women has been found to have the disease. It is the second most common cause of hypercalcemia in hospitalized patients (where malignancy is the leading cause). With the widespread use of auto-analyzers (which include a serum calcium and phosphorus) and the confirming parathormone ligand assays, the prevalence of this condition has been increasingly detected in asymptomatic patients being studied for other diseases. Most frequently, the source is a solitary benign parathyroid adenoma or hyperplasia that can be removed surgically.

Rationale for Surgery in Asymptomatic Patients

In current series, 10%–50% of patients are considered asymptomatic. There is a developing consensus that such patients should be operated on because there is no way of predicting who will develop complications and when. For example, demineralization of bone may occur suddenly (*1*). There is increasing evidence that, whereas parathyroidectomy prevents complications, it does not necessarily cure them once they are established. For example, demineralization of bone may never be reversed (*1*).

Parathyroid Surgeon's Viewpoint of Preoperative Imaging Methods in HPT

The experienced parathyroid surgeon finds the diseased glands in 92%–98% of patients at the first operation (*2*). All patients should have bilateral neck explorations to try to identify at least four parathyroid glands in order to detect and resect all double adenomas and asymmetric parathyroid hyperplasia.

In 5%–10% of patients after initial surgery, hypercalcemia persists or recurs. This persistence of disease after surgery occurs because either no pathologic source was found or not all the pathologic sources were removed.

Usually, the source is an ectopic adenoma. The ectopic adenoma is ususally in the carotid sheath or the tracheal–esophageal groove or in the thymus or the superior mediastinum. Figure 1 shows the normal and ectopic locations of normal parathyroid glands as summarized from anatomic studies (*3*).

Older patients have an increased incidence of double adenomas. In patients aged 65 and over, 9% have double adenomas. Unilateral exploration would miss 5% (*2*). Preoperative localization in HPT has not increased the cure rate (percentage of successful parathyroidectomies) nor decreased the morbidity or the duration of the initial operation.

The Future of Preoperative Localization in HPT

If operative policy, for any reason, should change so that the surgeon were to look for only one enlarged and one normal gland, or should a localization method develop that could localize all "normal" parathyroid glands reliably, noninvasive localization would decrease the duration of the operation and its morbidity (*4*).

We demonstrated the concentration of radiocyanocobalamine (CO57B12) in parathyroid glands in 1962 (*5*). The relative tissue concentration of CO57B12 was adequate to reveal parathyroid tissue when it was clearly separate from the thyroid area, but it was not high enough when the parathyroid adenoma was in the region of the thyroid (at operation 1 day after injection, in situ 1 mg parathyroid = 0.52, thyroid = 0.32, muscle = 0.01).

In 1964, we demonstrated successful parathyroid scanning in the human with Selenium-75-labeled methionine (*6*). In patients scanned preoperatively, with the subsequent removal of a parathyroid adenoma, a correct preoperative localization was made in five patients but not in eight cases. Three of the five correctly located adenomas weighed >3 g. All our failures were in patients with ade-

Received Dec. 20, 1990; revision accepted Mar. 19, 1991.
For reprints contact: William H. Beierwaltes, MD, St. John Hospital and Medical Center, 22101 Moross Rd., Detroit, MI 48236-2172.

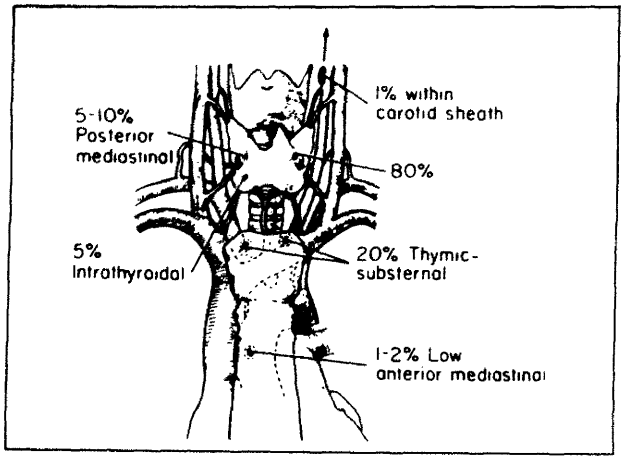

FIGURE 1. Normal and ectopic locations of normal parathyroid glands as summarized from anatomic studies (*3*).

nomas <1.4 g in weight. We summarized our work in 1968 in these approaches and with ^{131}I-labeled toluidine blue in humans (*7*). More recently, Zwas et al. (*8*) published better results with labeled toluidine blue than we were able to obtain, because of a better synthesis of toluidine blue, plus technetium 99m-pertechnetate subtraction imaging. Labeled amino acids have recently shown some promise with PET scanning (*4*).

Strengths and Weaknesses of Preoperative Localization in the HPT Patient Who Has Already Undergone One Parathyroid Operation

Thallium Technetium Scintigraphy. The patient is first injected with a tracer dose of radioactive thallium (thallium images for both thyroid and parathyroid tissue). After images of the anterior neck and superior mediastinum are obtained, a technetium thyroid scan is immediately obtained (technetium images the thyroid gland but not parathyroid tissue). When the technetium scan is subtracted from the thallium scan, a blank picture of the thyroid is seen with a radioactively "hot" area of thallium uptake in the parathyroid adenoma. The whole procedure takes less than 2 hr.

The primary virtue of scintigraphy is that its sensitivity and specificity are not decreased by the previous surgery. It has a sensitivity of about 75% and a specificity of 90%.

When the nuclear medicine physician is not certain that a parathyroid adenoma is present and uses the term "indeterminate" probability, the published sensitivity is 91%, with only one false-positive result (*4*).

The primary problem with scintigraphy is that thyroid gland abnormalities decrease the sensitivity and specificity. Unfortunately, a high percentage of patients with hyperparathyroidism have had X-irradiation of the head, neck, or chest as a child; these patients have a 23% incidence of colloid nodular goiter and a 7% incidence of thyroid cancer.

High-resolution ultrasound with a 10-MHz small-parts real-time scanner, in the hands of Stark et al. (*9*) detected benign thyroid lesions averaging 7 mm in size, a 5-mm follicular carcinoma, and a 20-mm recurrent medullary carcinoma in patients with HPT.

We have also had posteriorly located glands missed by scintigraphy, regardless of size. We have detected some mediastinal adenomas as well as some small cervical adenomas (300 mg). In some patients with hyperplasia or double adenomas, only one enlarged gland has been detected (*2*).

Scintigraphy should identify >90% of adenomas that are ≥500 mg in size, most of which were 300–500 mg in size. Most adenomas <300 mg are seen. An adenoma as small as 60 mg has been detected (*4*). The technique is less sensitive in detecting secondary parathyroid hyperplasia. An intrathyroidal parathyroid adenoma has been detected. The nonspecificity of the uptake has led to an ever-increasing list of false-positive results, which include a sarcoid lymph node, primary thyroid carcinoma, metastatic carcinoma, and Hodgkin's lymphoma (*4*). The specificity of the procedure is almost totally dependent on patient selection. For example, specificity is highest when the use of the scan is limited to patients with biochemically confirmed hypercalcemia and elevated serum parathyroid hormone (PTH) levels. It is also higher in patients who are symptomatic. It is less altered by previous operative changes than ultrasound and computed tomography (CT) scanning.

Ultrasound. Ultrasound is at its best in detecting adenomas around the lower pole of the thyroid. However, adenomas around the lower pole of the thyroid are the easiest for the surgeon to find. Ultrasound is at its worst in detection of retrotracheal, retroesophageal, and mediastinal adenomas. Ultrasound is not competitive for ectopic adenomas in either the posterior or the superior mediastinum.

In practice, the most successful results are frequently related to one particular individual who is using one particular technique enthusiastically and getting feedback on each of his or her results. In community hospitals, this is frequently a radiologist specializing in ultrasound in one hospital in the city who is highly motivated to specialize in parathyroid adenoma detection.

CT Scans. The CT scan can visualize retrotracheal, retroesophageal and mediastinal parathyroid adenomas. CT is best for mediastinal adenomas. CT has difficulty in the neck and shoulder regions due to swallowing and bone artifact, but these artifacts are being reduced with better patient preparation and fast scanners. There is a questionably acceptable morbidity in the use of CT with intravenous contrast. Neither CT nor ultrasound has reduced the incidence of re-operation when used for pre-operative screening and localization.

MRI Scan. Magnetic resonance imaging (MRI) is about 75% sensitive and more expensive than CT and ultrasound. MRI surface coils have improved resolution in the

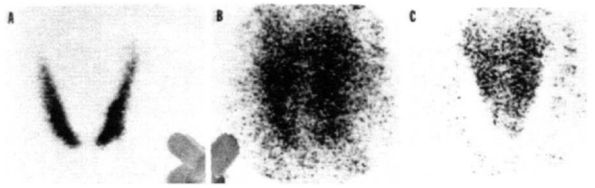

FIGURE 2. (A) Technetium scan in a patient with no parathyroid disease. (B) Thallium scan. (C) Subtraction scan. No parathyroid adenoma is seen.

neck. MRI cannot distinguish parathyroid adenomas from hyperplasia or thyroid disorders. It has a high cost and low specificity.

Selective Venous Parathormone Sampling and Arteriography. Selective venous parathormone sampling and arteriography are used less often because they are more invasive, expensive, and lack sensitivity.

Experience in Parathyroid Scintigraphy in Community Hospitals. Figure 2A shows a technetium scan in a patient with no parathyroid disease (at St. John Hospital in Detroit). Figure 2B shows the thallium scan on the same patient. Figure 2C shows the subtraction scan with no localization of parathyroid adenoma.

Figure 3 is a subtraction scan scintigraphy on a 64-yr-old woman at St. John Hospital on 5/26/84. She had a malignant hypertension and an increased total calcium and increased parathormone. Her scan showed a surgically proved 2-cm diameter parathyroid adenoma at the medial aspect of the right lobe.

In a recent review of scintigraphic parathyroid imaging at William Beaumont Hospital (Royal Oak) on 21 patients studied between 7/1/87 and 3/31/89, the sensitivity was found to be 83%, specificity 100%, and accuracy 98% (data provided courtesy of A. Ballingit and H. Dworkin).

ADRENAL CORTEX AND OVARIES

Origin and First Use of Iodocholesterol

In 1970, we published the origin of [^{131}I]19-iodocholesterol (NP-55) (*10*). In April 1971, we published the first visualization of the human adrenal in vivo by scintigraphy with NP-55 (*11*). In December 1971, we published in the *New England Journal of Medicine* the first diagnosis of human adrenal disease by visualization of the adrenal glands with NP-55 (*12*). Figure 4B shows the structure of NP-55. Kojima, in Japan, found a contaminant in NP-55

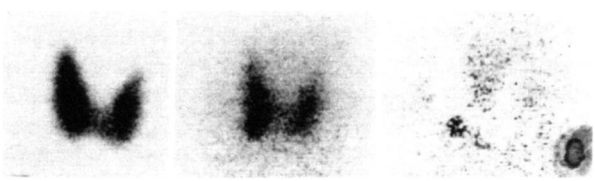

FIGURE 3. Subtraction scan showing a surgically proved 2-cm diameter thyroid adenoma at the medial aspect of the right lobe.

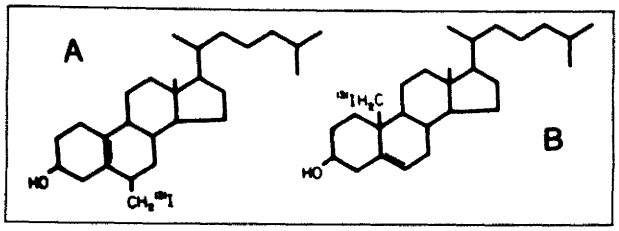

FIGURE 4. (A) The structure of ^{131}I-19-iodocholesterol (NP-55) and (B) 6-Beta iodomethyl-19-nor cholesterol (NP-59) (*35*).

(^{131}I-6-β-iodomethyl-19-nor-cholesterol) (Fig. 4A), which showed a higher uptake in the adrenal cortex than NP-55. This agent was synthesized simultaneously by Kojima and our group (*13,14*). We showed the superiority of this agent (NP-59) to NP-55 in 1975 in humans (*15*). NP-59 showed a five-fold higher concentration in the adrenal cortex and higher target-to-nontarget ratios than NP-55 with subsequent improvement of adrenocortical images. Since then, the University of Michigan Nuclear Medicine Pharmacy has been supplying NP-59 throughout the United States.

We have published several articles on newly synthesized radiolabeled enzyme inhibitors (*16–19*) that image the adrenal cortex much more quickly and with a much lower radiation dose, but none of these have proved to be practical in the human to date.

Use in Cushing's Syndrome

ACTH Excess Versus Adrenocortical Adenoma. The most popular use of NP-59 has been in the differential diagnosis of Cushing's syndrome. Here it is most helpful in differentiating between ACTH overstimulation of both adrenal cortices versus adrenocortical adenoma overfunctioning. Basically, ACTH excess scintigrams show good uptake in both adrenals (Fig. 5A), while adrenal adenoma scintigrams show uptake in only one adrenal (Fig. 5B) because the cortisol produced by the hyperfunctioning adenoma suppresses the pituitary stimulation of the rest of the two adrenals with ACTH.

Table 1 shows the four different types of scan interpretation. Gross et al. (*20*) reported our experience in Helsinki, August 1984. We had used iodocholesterol imaging on 490 patients over 8 yr (1976–1984); The results showed that 160 of these patients had CS; 157 patients had hyperaldosteronism; and 119 of these patients had adrenal hyperandrogenism. Three of these patients were false-positive and six were false-negative. Gross et al. later reported our experience with 75 patients with CS who had iodocholesterol, CT, and angiography in which a final diagnosis was available at the University of Michigan between 1971 and April 1985 (*21*). It was found that 84% had ACTH-dependent disease, and 16% had ACTH-independent disease. Seven of these were adenomas, two were cortical nodular hyperplasia and one had both ACTH-dependent and ACTH-independent disease.

Early Use. In 1974 we demonstrated in two patients without CS that nodules of the human adrenal cortex not

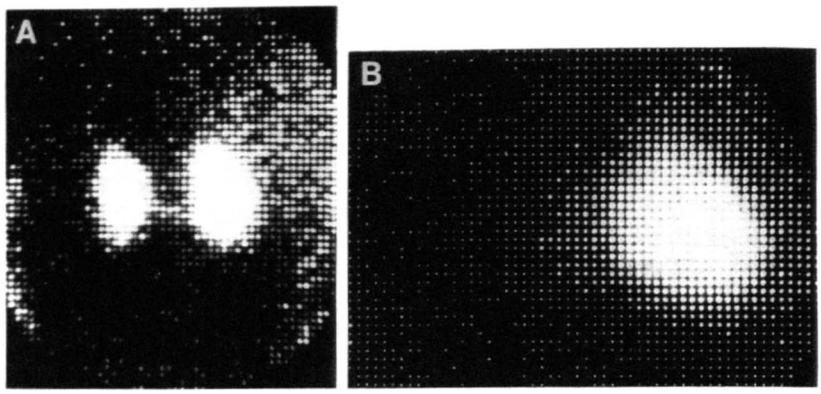

FIGURE 5. (A) Posterior adrenal control scintigram in ACTH-dependent bilateral adrenal hyperplasia due to a pituitary adenoma (*77*). (B) Posterior adrenal corticol scintigram of an adrenal adenoma in a patient with CS. The normal cortex is not imaged because of suppression of pituitary ACTH.

previously known to be functional were functional (*22*). One patient had a radioactive hot nodule, not suppressible with dexamethasone in one adrenal gland with suppressed uptake of NP-55 in the contralateral adrenal cortex. She had a normal response to ACTH stimulation of the opposite adrenal gland. Figure 6 presents the iodocholesterol adrenal gland image of the first patient without treatment (Fig. 6A), after dexamethasone suppression (Fig. 6B) and after ACTH stimulation (Fig. 6C). This sequence is identical to that in patients with CS secondary to an autonomous hyperfunctioning adrenocortical adenoma.

The second patient had a hot nodule in one adrenal gland that was suppressible with dexamethasone; ACTH produced normal uptake in the opposite adrenal gland. We pointed out the similarity of the functional nodules in the adrenal cortices to functional nodules in the thyroid gland with ^{131}I. We also pointed out the possible similarity of some cases developing CS (cortisol producing nodules) to Plummer's disease thyrotoxicosis (thyroxine-producing nodules) in the thyroid gland. Since this report, our observations have been confirmed in several institutions.

Correlation of NP-59 Percentage Uptake with Conventional Endocrine Tests. We then published a series of papers relating the correlation of percentage uptake with conventional endocrine tests (*23–26*). This work was made possible because of our early conviction that the percentage uptake test in the adrenal cortex with iodocholesterol would be as important an estimate of hyperfunction as the Na ^{131}I percent uptake in the thyroid to estimate the degree of function of the thyroid gland (*27,28*).

A 0.97 correlation coefficient between NP-59 percentage uptake and urinary-free cortisol was demonstrated in patients with CS (*23*). The 24-hr urinary free cortisol was generally considered the best screening test for CS. There was no good correlation between the iodocholesterol uptake and the plasma cortisol, the plasma ACTH, the cortisol secretion rate, and the urinary 17-hydroxysteroids and the urinary 17-ketosteroids. We believe that it is because these are spot tests.

Most recently Geatti et al. (*29*), from the University of Michigan Nuclear Medicine Division, reported correct localization by NP-59 functional scintigraphy of an adrenocortical adenoma causing CS after US and CT scan had failed to show any abnormality of the adrenal glands.

Detection of Relapse of CS After Relief of Cushing's Disease After Pituitary Irradiation. NP-59 also detects recurrence of ACTH excess after pituitary X-ray therapy and during mitotane therapy for ACTH-dependent Cush-

TABLE 1
Imaging Patterns in Cushing's Syndrome

Scintigraphic pattern	Form of CS
Bilateral symmetric	ACTH dependent
	Hypothalamic
	Pituitary
	Ectopic ACTH syndrome
Bilateral asymmetric	ACTH independent
	Nodular hyperplasia
Unilateral	Adrenal adenoma
	Adrenal remnant (ectopic adrenocortical tissue)
Bilateral nonvisualization	Adrenal carcinoma (functioning tumor suppresses contralateral gland)

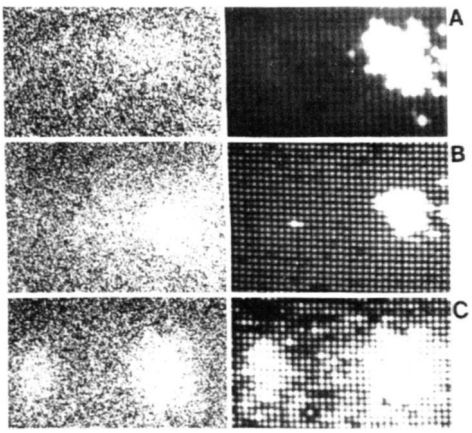

FIGURE 6. Iodocholesterol image of a patient without CS (posterior view). (A) Without treatment. (B) After dexamethasone suppression. (C) After ACTH stimulation. This sequence is identical to that in patients with CS secondary to an autonomous hyperfunctioning adrenal cortical adenoma (*22*).

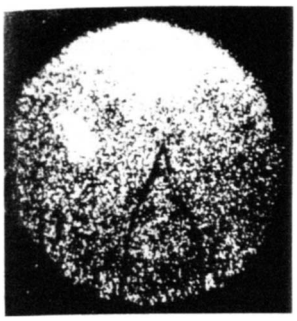

FIGURE 7. Functioning adrenal autotransplant under skin of right thigh (but not in left thigh) of a patient 1 yr after bilateral "total" adrenalectomy, and transplants under the skin of both thighs.

ing's disease of pituitary origin (*30*). When such a patient is properly controlled on this therapy, the adrenals are not imaged with NP-59 (>50% suppression of uptake). We scan such patients at 3-mo intervals. Reappearance of imaging of the adrenals with NP-59 may be detectable before a diagnostic rise in the serum ACTH or recurrence of symptoms (*30*).

Detection of Adrenocortical Remnants Causing Persistent or Recurrent Cushing's Disease after Bilateral "Total" Adrenalectomy. NP-59 will detect the remnants so that they can be successfully removed surgically, when all other methods of localization have failed (*31,32*). This is possible because NP-59 detects adrenocortical function specifically, whereas the CT scan and ultrasound (US) merely measure differences in tissue density. The detection of a mass by CT or US does not prove that it is hyperfunctioning adrenocortical tissue. Under these circumstances, the NP-59 location of remnants (which the surgeon has been unable to find during previous operations) is also made possible by calibration of the pixels in millimeters on the digitized image. A radioactive source strip on the patient's back allows calculation of depth from the posterior skin surface using the radioactive line source on the back in the left lateral projection. Thus, a two-dimensional fix in millimeters guides the surgeon.

Evaluation of Adrenal Autotransplant After Bilateral Total Adrenalectomy for Cushing's Disease. NP-59 has also been used here to evaluate the viability of adrenal autotransplants resected and reimplanted under the skin of the thigh in patients with Cushing's disease (*33, 34*). In this situation, again the physician is not interested in whether a mass is present, which might be demonstrated by CT or US, but in whether the mass is functional (Fig. 7).

Aldosteronism and Low-Renin "Essential" Hypertension

Differentiation Among Adenoma, Macronodular Hyperplasia, and Micronodular Hyperplasia. The syndrome of primary aldosteronism is characterized by hypertension, hypokalemia, hypernatremia and metabolic alkalosis (*35*). Serum and urinary aldosterone levels are elevated and plasma renin activity is suppressed. This disorder results from an autonomous tumor (usually a benign adenoma) in two-thirds of cases and from bilateral hyperplasia in one-third. Hypersecretory adenomas are best treated surgically, and bilateral hyperplasia by medical means.

Since aldosterone does not significantly suppress ACTH output from the pituitary (as cortisol does), we developed the use of dexamethasone to enhance the sensitivity and accuracy of adrenal cortical scintigraphy in this disease (*36–38*). In 1976, we compared the results of adrenal scintiscan, venogram, and venous aldosterone levels with the histologic findings in 33 patients submitted to operations at the University of Michigan Hospital for primary aldosteronism. The adrenal lesions were histologically classified into four categories: 25 patients had adenomas (Fig. 8A), 6 had macronodular hyperplasia (Fig. 8B), 1 had microscopic hyperplasia (Fig. 8C), and one had an adenocarcinoma. Asymmetric uptake between the two adrenals seen on standard scan (without dexamethasone suppression) did not differentiate between a tumor or asymmetrical hyperplasia, unless the tumor was greater than 2 cm in diameter. During suppression scintiscans, unilateral uptake visible in less than 5 days after the tracer injection was consistent with adenoma. Patients with nodular hyperplasia demonstrated uptake in both adrenal glands in less than 5 days. The patient with microscopic hyperplasia took more than 4 days to image bilaterally on dexamethasone suppression.

The type of adrenal lesion was correctly identified in 20 of 26 (77%) of patients by suppression scintiscans; in 21 of 28 (75%) of patients by venograms, and in 12 of 16 (75%) of patients who had adrenal venous aldosterone measurements attempted. We concluded that adrenal vein catheterization can be reserved for those patients in whom the results of suppression scintiscans are inconsistent with the clinical degree of aldosteronism (*38*). Figure 9A shows an adenoma in the right adrenal at Day 3 with dexamethasone suppression. The normal adrenal shows breakthrough imaging at Day 5. Under the same circumstances, Figure 9B shows breakthrough imaging at Day 3 in a

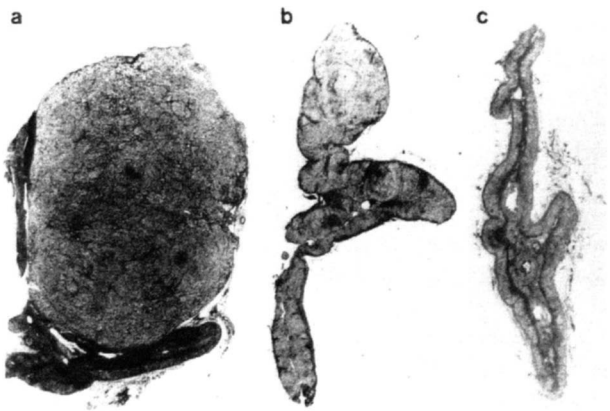

FIGURE 8. Histopathology of (A) adenoma, (B) macronodular hyperplasia, and (C) micronodular hyperplasia in patients with hyperaldosteronism (*38*).

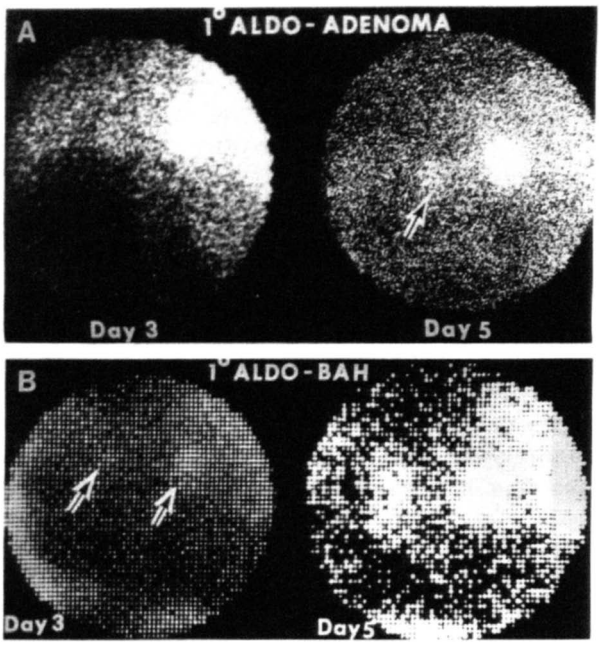

FIGURE 9. (A) Posterior NP-59 dexamethasone-suppression adrenal scintiscan in a patient with primary aldosteronism due to an adrenal adenoma. Day 3 study identifies the adenoma. Day 5 image shows the adenoma and the normal adrenal cortex (arrow). (B) Posterior dexamethasone-suppression adrenal scintiscan in a patient with primary aldosteronism due to bilateral adrenal macronodular hyperplasia. Day 3 study shows early uptake. Day 5 study confirms the Day 3 findings.

patient with bilateral macronodular hyperplasia, more intense at day 5. Using our later NP-59 and a single photon tomographic scanner, Mayo Clinic workers (*39*) reported the detection of 100% of aldosteronomas with NP-59 within as little as 24 hr after administration of the tracer.

Low-Renin "Essential" Hypertension

Classic hypokalemic primary aldosteronism, due to either aldosteronoma or benign hyperplasia, accounts for less than 1% of all hypertension. However, it is now established that approximately 30% of the hypertensive population has abnormally low plasma renin activity, and there is substantial evidence that a significant percentage of patients with benign "essential" hypertension have underlying functional and histopathologic abnormalities of the adrenal (*40*). In a highly selected series of 130 hypertensive patients referred for evaluation, Gunnels and coworkers (*40*) found 32 with low plasma renin activity and clearly subnormal response to restricted salt intake and diuretic administration. Of these, 14 had hypokalemic aldosteronism. The remaining 18 demonstrated variable patterns of aldosterone secretion and serum potassium levels but did not fulfill the diagnostic criteria for classic primary aldosteronism. All patients were explored surgically and the same range of histopathology (i.e., diffuse hyperplasia, micronodular and macronodular hyperplasia, and adenoma) was found in both groups. Although the patients with adrenal adenoma and/or hyperplasia who met the criteria for hypokalemic aldosteronism demonstrated the best blood pressure response to adrenalectomy, blood pressure improved postoperatively in 82% of the remaining patients (*40*).

Initial results of adrenocortical DS scintiscanning in patients with low renin "essential" hypertension have supported the above observations (*41*). The same types of scintigraphic patterns have been observed as in primary aldosteronism. One patient who had a venographically proven adenoma demonstrated asymmetrical uptake by DS scanning. Seven of nine patients who demonstrated early bilateral visualization on DS scans have responded well to spironolactone therapy. On the other hand, poor response to spironolactone has been found in hypertensive patients with normal adrenal suppression. These are admittedly preliminary results, but they are intriguing and suggest a potential new role for adrenal scintigraphy.

Correlation of Percentage Uptake with Urinary Aldosterone Excretion

We demonstrated that 50% of the uptake of NP-59 was ACTH dependent (dexamethasone suppressible), and 10% was angiotension II-dependent (suppressible with high salt diet). Regulation of the "residual" 40% of the uptake is unknown but is probably related to low-density lipoprotein receptors (*24*).

We determined the relationship of NP-59 adrenal percentage uptake 5 days after radiotracer injection to 24-hr urinary aldosterone excretion in primary aldosteronism patients (*25*). The correlation coefficient was 0.93. The correlation coefficient of uptake to urinary aldosterone excretion in patients with bilateral adrenal hyperplasia is only 0.60 (*25*).

Our current approach (*24*) to the problem of primary aldosteronism has been dexamethasone suppression 4 mgm daily for 7 days before the injection and daily through the period of imaging (*42*), with NP-59 scintigraphy on the third and fifth days after the injection in patients proved to have the biochemical abnormalities of this disorder. Unilateral NP-59 uptake may be sufficient to lead to surgical intervention, given the accuracy of diagnosis for adenoma using scintigraphy. However, a complementary study of anatomy using a technique such as CT or MRI may be performed to delineate the relationship of the tumor to other structures (*43*). This is seldom indicated in cases of hyperplasia revealed by bilateral early imaging patterns, in which confirmatory adrenal vein sampling of aldosterone levels has been used to confirm the scintiscan results (*43*).

Most recently, Nomurs et al. (*44*) found that all of 19 cases had a higher NP-59 uptake on the adenoma side than on the opposite side when a two-fold difference was the criterion for lateralization. Two patients were false negative because of ratios of 1.3 and 1.2 with adenoma

volumes of 1.1 and 1.2 cm^3 volume, while adenomas as small as 0.5 cm^3 were detected with ratios of 3.5 (adenoma/opposite adrenal).

MRI has the potential to detect adenomas based on changes in signal intensity in addition to contour distortion. Aldosteronomas in MRI show slightly increased signal intensity compared with that from liver on long-TR/TE sequences.

Adrenal Hyperandrogenism and Hirsutism

We were pleased to demonstrate (*45*) that the results in adrenal scintiscanning in hirsutism and hyperandrogenism were similar to scintiscanning in aldosteronism in that adrenocortical adenomas and hyperplasia (but in the zona fasciculata and reticularis, rather than in the zona glomerulosa) could be detected. It also required dexamethasone suppression scanning because androgens (like aldosterone) have little suppressive effect on pituitary and hypothalmic ACTH secretion (*45*). In this effort, we also reported the first androgen secreting adenoma in the MEA type 1 syndrome and its detection by adrenal scintigraphy (*45*). Everyone working in a nuclear medicine thyroid clinic soon becomes aware of the frequency of the problem of hirsutism (*46*).

The innermost adrenocortical layer synthesizes adrenal androgens that are of low potency (dihydroepiandrosterone, androstenedione), but that, if secreted in excess, can lead to hirsutism and virilization, with characteristic features of temporal balding, oligomenorrhea or amenorrhea, increased muscle mass, and clitoromegaly. This may be a consequence of autonomous tumors (adenoma or carcinoma) or hyperplasia caused by inborn or acquired abnormalities of adrenocortical hormone biosynthesis.

The patterns of adrenal imaging seen in adrenal hyperandrogenism are similar to those in primary aldosteronism, with early (prior to the fifth day) unilateral imaging of adenomas, which are relatively rare lesions (Fig. 10),

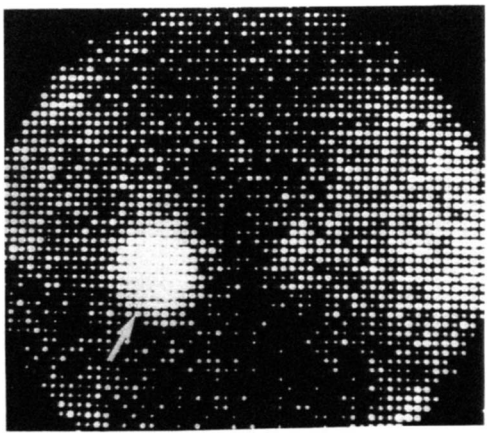

FIGURE 10. Posterior NP-59 dexamethasone suppression adrenal scan in hyperandrogenism due to an adrenal adenoma (arrow). The normal contralateral cortex is faintly seen, as this image was obtained 5 days after the tracer injection (*45*).

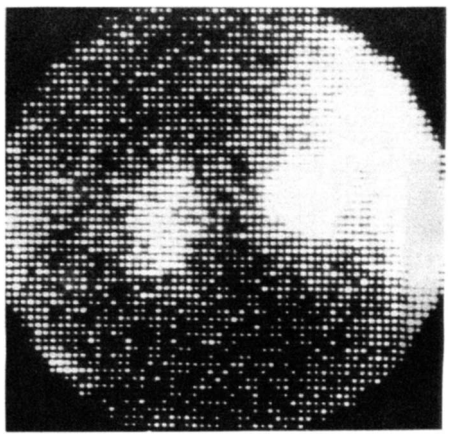

FIGURE 11. Posterior NP-59 dexamethasone suppression scan in hyperandrogenism due to bilateral adrenal hyperplasia (*45*).

and early bilateral imaging in bilateral adrenal hyperplasia (Fig. 11). The latter is seen in congenital adrenal hyperplasia (CAH) due to enzymatic deficiencies, but in these cases the diagnosis usually is best made by measurement of high levels of 17-hydroxyprogesterone and other metabolites.

The so-called polycystic ovarian (PCO) syndrome is associated with various degrees of hirsutism and virilization in which androgen excess from the ovary has been demonstrated. A significant portion of PCO patients also have an abnormality of adrenal androgen secretion (*47*). This abnormality can be unequivocally demonstrated only by simultaneous adrenal and ovarian vein catheterization and blood sampling for androgen assay. An alternative to this invasive technique is adrenal scintigraphy, which has been used to demonstrate the presence of an adrenocortical abnormality manifested as excessive NP-59 uptake in a number of patients with the PCO syndrome (*47*). As in the case of hypersecretion from the other two layers of the cortex, we have demonstrated that adrenal NP-59 uptake in conditions of adrenal androgen hypersecretion correlates with 17-ketosteroid excretion rates, a measure of this hyperfunction in both adrenal adenoma and bilateral hyperplasia (*26*).

Correlative adrenal imaging using both CT and MRI may prove useful. Primary adrenal tumors causing virilizing syndromes usually are large and therefore detectable with MRI. In CAH, there is usually gross adrenal enlargement that is easily detected on MRI. As in other endocrine disorders with adrenal hyperplasia attributable to chronic exposure to elevated ACTH levels, MRI is not able to detect an abnormal change in signal intensity. Because virilization is often a childhood disease, MRI or US might be preferable to CT in this group of patients to exclude a possible adrenal tumor (*48*).

Ovarian Tumors Causing Masculinization

Isolated instances of radioiodinated cholesterol uptake by virilizing tumors of the ovary (sometimes large and

missed by pelvic examination) have been reported, and scintigraphic examination of the pelvis may have utility in those cases in which no adrenal abnormality can be observed with CT or US (*49,50*).

"Incidentalomas": Distinguishing Benign from Malignant Eu-adrenal Masses

The most common use of iodocholesterol, however, today is in the detection of the "incidentaloma." These are endocrinologically silent masses detected by high resolution CT scanning of the upper abdomen for reasons not related to the adrenal. Figure 12B is a scan of our first incidentaloma, consisting of a hemorrhage underneath the capsule of the liver. The CT scan shows a huge tumor (Fig. 12B). The iodocholesterol scan images both adrenals normally but shows a cold spot in the region of the liver imaging posteriorly (Fig. 12A).

Gross et al. (*51*) in our department of nuclear medicine, studied endocrinologically silent masses. High-resolution CT detects such masses in 1%–10% of patients. These masses (both microscopic and macroscopic) have been found in 2%–9% of patients at autopsy. Many physicians had adopted the philosophy that most of those adrenal tumors >5 cm were malignant and therefore any over 3 cm in diameter should be resected. Needle aspiration did not give reliable pathology. It also had a significant morbidity and mortality. The majority of these removed tumors were benign.

Gross et al. (*51*) published a follow-up study of 119 eu-adrenal patients with unilateral adrenal masses on CT scan for nonadrenal complaints ("incidentaloma"). The mean diameter of these lesions was 3.3 cm ± 1.9 cm. In 76 patients, the iodocholesterol uptake on the side of the adrenal mass was "concordant." All had an adenoma with a mean diameter of 2.8 ± 1.2 cm. In 26 patients with decreased uptake on the side of the mass (discordant) the mean diameter was 4.1 cm ± 2 cm. Nineteen of these were metastatic malignancies. Four were primary malignancies. Three were cysts. In 12 patients with bilateral symmetric uptake, 2 were metastatic and 6 were adenomas less than 2 cm in diameter. Four were periadrenal. These consisted of gastric varix, hematoma, and a myelolymphoma. Five were pseudoadrenal (renal cyst, gastric leiomyoma). The sensitivity of the iodocholesterol scan was 76%. False-negatives were present in six presumably because they are less than 2 cm in diameter. The specificity was 100%. There were no false-positives. The accuracy was 93%. The predictive value of the positive test was 100%.

Thus, although this problem is still under active study, those lesions that demonstrate significant NP-59 uptake are benign and may be observed, whereas lesions that fail to accumulate NP-59 or that distort the normal pattern of adrenal NP-59 uptake require further investigation. The potential of MRI tissue characterization may also have a role in the investigation of such lesions. The high water content of pheochromocytomas and metastatic deposits, as compared with the content in more lipid-laden adrenocortical adenomas, may be distinguished by this technique.

Benign nonhyperfunctioning adenomas on MRI produce a low signal intensity on spin-echo (SE) sequences with a short TR and a moderate or low signal intensity on SE sequences with a long TR (*48,51*). However, nonhyperfunctioning adenomas may show necrosis, hemorrhage, and cystic changes, in which case signal-intensity observations can be equal to those from metastasis, functioning lesions, or cysts. Most incidental adenomas (90%) produce signal intensity equal to that from the liver, whereas other adrenal masses, including cystic lesions and metastasis, produce signal intensity higher than that from liver. However, because overlap in signal intensity between benign and malignant masses does occur in up to 25% of cases, a presumable benign silent mass must be monitored by follow-up studies to exclude the possibility of low-signal-intensity metastasis (*48,51*).

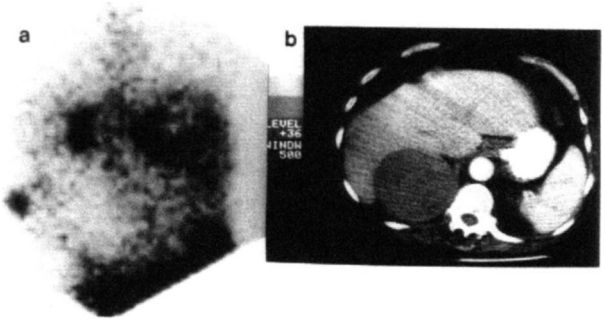

FIGURE 12. Posterior NP-59 scintigram visualizing both adrenal glands normally (a). The "tumor" was a subcapsular hematoma in the liver. Scan shows "cold" spot in the liver in that location (a). CT scan showing a large tumor in the region of the right adrenal gland (b).

ADRENAL MEDULLA IMAGING

Metaiodobenzylguanidine

My history of the development of imaging of chromaffin-granule containing tumors has been published (*52, 53*). Our first publication in 1967, evaluating ^{14}C-labeled precursors of melanin to develop a radiopharmaceutical for the diagnosis and treatment of malignant melanomas, surprised us by showing that ^{14}C-labeled dopamine showed the highest uptake in the adrenal medulla of dogs and that the runner-up was norepinephrine (NE). Nineteen years and 37 directly-related publications later we received our patent (*54*). The molecular structure of metaiodobenzylguanidine (MIBG) has some similarities to the adrenergic hormone-neurotransmitter, NE (Fig. 13).

NE is synthesized by normal adrenergic neurons and adrenal medulla cells, stored in adrenergic granules, and secreted by exocytosis. Some of the secreted NE is taken up by the same adrenergic cells and stored again in gran-

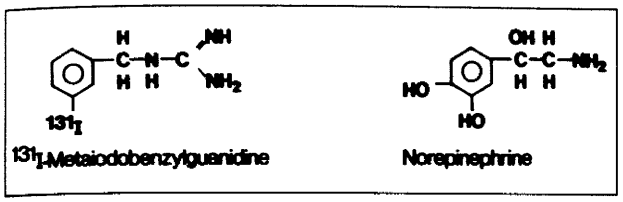

FIGURE 13. Similarities of molecular structure of MIBG compared with that of norepinephrine.

ules. It is this uptake process that enables MIBG to enter into the pathways of NE into and out of adrenergic tissues. Radiolabeled MIBG differs from NE in that the radiopharmaceutical binds little to post-synaptic receptors, causes little or no pharmacologic response in tissue, and is metabolized to only a modest extent. The uptake, storage, and release of NE and MIBG take place in the chromaffin granules. Conceptually, the chromaffin granule has potential for the highest "specific uptake" and the highest imaginable target-to-nontarget ratio. A single chroffin cell contains about 30,000 chromaffin granules or vesicles (*55*). Within the vesicle, the concentration of epinephrine is 25,000 times the concentration in the cytosol, testifying to the efficacy of the transport mechanism (*52*). Figure 14 is a microphotograph of a cut section of a chromaffin cell showing the large numbers of chromaffin granules (*55*).

Adrenal Medullary Hyperplasia

Our first diagnostic use of MIBG in human beings was in patients with the MEN-IIa and MEN-IIb syndromes, who would be expected to have bilateral adrenal medullary hyperplasia (*56*). Whereas the adrenals are imaged transiently with 0.5 mCi of MIBG in only a small percentage of normal controls, in patients with an enlarged adrenal medulla from MEN-IIa and MEN-IIb it is characteristic that definite imaging of the adrenal occurs throughout the 3-day period of examination after the tracer dose is administered. When one cuts through a normal adrenal to produce a cross-sectional specimen, the normal adrenal

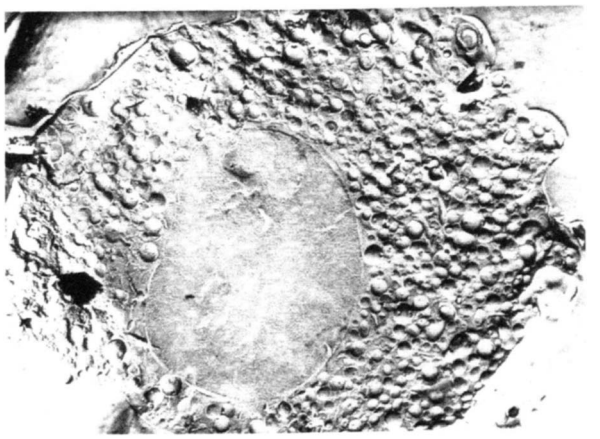

FIGURE 14. Microphotograph of a cut section of a chromaffin cell showing the large numbers of chromaffin granules (*55*).

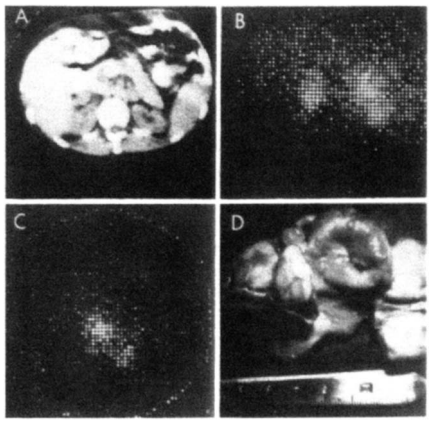

FIGURE 15. Posterior view MIBG imaging of both adrenals (B) in a patient with a relative photon-deficient area between these two, as shown by pinhole imaging of right adrenal (C). The CT scan was nondiagnostic (A). Subsequent removal of the right adrenal disclosed (D) that the upper hot spot was a functional pheochromocytoma. The middle photon-deficient area was an area of necrosis and hemorrhage, and two pheochromocytomas are seen below this area (*80*).

cortex to medulla ratio is about 10:1. As the adrenal medulla enlarges, it enlarges at the expense of the adrenal cortex. Computed tomography (CT) and nuclear magnetic resonance (MRI) therefore may be unable to detect adrenal medullary hyperplasia until it is so advanced that the ratio of cortex to medulla is reversed to 1:10. Within this hyperplasia, micronodules first form, then macronodules; when the macronodules are 1 cm in diameter or larger they are called pheochromocytomas.

Figure 15 shows bilateral MIBG adrenal imaging (B) in a patient with an MEN-IIb who also appears to have one hot spot in the left adrenal and two hot spots in the right adrenal with a relative photon-deficient area between these two (C, pinhole view of right adrenal). The CT scan in this patient was nondiagnostic (Fig. 15A). Surgical removal of the right adrenal disclosed that the upper hot spot (Fig. 15D) was a functional pheochromocytoma and the middle photon-deficient area was an area of necrosis and hemorrhage in a previously functioning pheochromocytoma; one functional pheochromocytoma was found below this region.

Pheochromocytomas

The CT scan is very sensitive in detecting tumors of the adrenal gland. However, it cannot tell the physician whether the tumor is a pheochromocytoma; it merely indicates that a mass is present that might fit the picture of a pheochromocytoma if the clinical data are suggestive. As shown in Figure 16, the MIBG scan proves that the mass found by CT scanning is a pheochromocytoma because it has "specific uptake"; i.e., MIBG is concentrated in catecholamine storage vesicles.

Scanning with CT is relatively insensitive in detecting extra-adrenal pheochromocytomas elsewhere in the abdomen or the chest. The MIBG scan is outstandingly

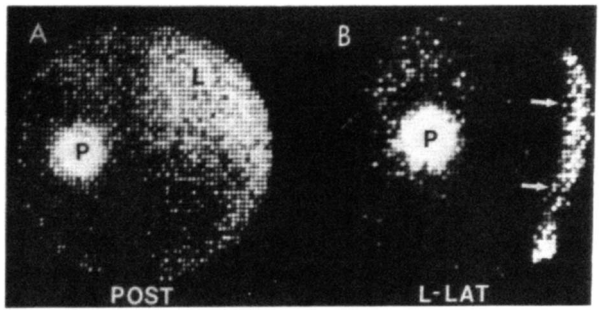

FIGURE 16. MIBG imaging of a mass anterior to and at the superior pole of the left kidney detected by CT scanning. The MIBG scan proves that the mass is a pheochromocytoma because of "specific uptake" in catecholamine storage granules in this neoplasm (*79*).

sensitive in localizing pheochromocytomas in both of these areas.

Chest. Figure 17, a posterior view of the MIBG scintiphotograph of the chest, shows the sharp localization of a pheochromocytoma in the upper cardiac region of the mediastimum of a 20-yr-old woman. In 1977 this woman had the classic picture and laboratory evidence diagnostic of a pheochromocytoma. In 1978 she underwent extensive invasive and traumatic studies at two respected medical centers. These investigations included intravenous pyelography (IVP) and nephrotomography; arteriography in the abdomen twice, in the pelvis once, and in the chest once; blood sampling from the vena cava on three differnet occasions; CT scanning of the chest and abdomen; tomography of the mediastinum and mastoids; and, finally, exploratory laparotomy. The results of all these studies were nonconfirmatory yet the plasma NE concentration was diagnostic at 16,000 pg/ml (<300 pg/ml). After successful MIBG scintigraphy, thoractomy resulted in the successful removal of a pheochromocytoma; the patient's symptoms disappeared and her plasma and urinary catecholamine levels reverted to normal.

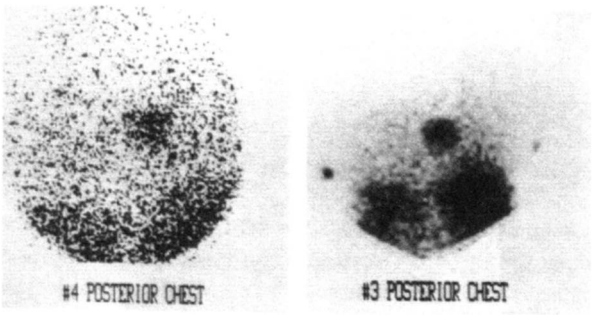

FIGURE 17. MIBG imaging of a pheochromocytoma in the region of the upper part of the heart in the mediastinum of a 20-yr-old woman. This tumor was not detected by a wide variety of imaging and invasive procedures.

Abdomen. Figure 18 shows the posterior abdominal MIBG scan localizing two areas of uptake between the kidneys (imaged with diethylenetriamine penta-acetic acid and superimposed on the adrenal scan) of a 30-yr-old patient. In this instance, residual pheochromocytoma tissue was detected postoperatively when the patient had persistent catecholamine excess. The patient had an 18-mo history of hypertension. A left adrenal pheochromocytoma 4×6 cm in size was resected at the University Hospital in Ann Arbor. He was asymptomatic for 6 mo, but all of the original symptoms then recurred. The plasma and urinary catecholamine levels became diagnostic of a pheochromocytoma. While taking phenoxybenzamine for treatment, the patient underwent chest and abdominal CT, abdominal ultrasonography, and vena cava sampling. The findings in all these studies were nonlocalizing.

The tissue near the left kidney was only 4 mm in diameter and was a persistent or recurrent pheochromocytoma, whereas the tissue near the right kidney was 2 cm in diameter. When the pixels are calibrated, these images give the surgeon a two-dimensional fix, so that even though he does not find the pheochromocytoma in the retroperitoneal area at surgery, he can press his thumb over the suspected area to see whether it causes a slight elevation in the blood pressure. If so, the tissue in that area can be removed and then inspected for pheochromocytoma, as in this patient.

Malignant Potential of Pheochromocytoma: Implications for Follow-up

Of 176 patients with pheochromocytoma studied at the University of Michigan during the past 5.5 yr, 46% had metastases (*53,57*), compared with the 10% rate usually reported (*58*). For all 176 patients, a review was made of the original histopathology and repeated plasma and urinary catecholamine measurements and MIBG scintigraphy were carried out; findings were compared with those of other imaging and localizing modalities (*57*).

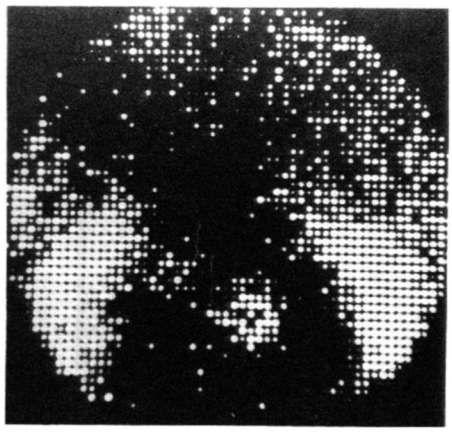

FIGURE 18. Posterior view MIBG imaging between the kidneys (imaged with ^{99m}Tc-DTPA) of pheochromocytoma remnants weighing 0.2 g (left) and 7.4 g (right). These were not detected by CT scanning.

In a previous publication reporting results from the first 400 patients who came to us for imaging of pheochromocytomas with MIBG, the sensitivity of MIBG imaging for malignant pheochromocytomas was 92.4% and the specificity was 100% (*59*).

Our criterion for the diagnosis of malignant pheochromocytoma was the presence of metastases in the liver, bone, lymph nodes, and lungs. A review of data on these 176 patients showed that in roughly one-half of cases (95 patients), metastases have not been detected to date. In the other one-half, however, metastases were detected, in 38 at the time of the primary operation. Review of the histopathology in all 176 patients showed no statistically significant histopathologic differences among them. Because of these observations, we have begun to obtain yearly MIBG scans on all those who undergo primary surgery for removal of a "benign" pheochromocytoma.

Imaging in the Treatment of Malignant Pheochromocytoma (62–64)

I have summarized and presented illustrations of this use of MIBG in my James L. Quinn III Memorial Essay (*53*) and will omit this topic from further discussion.

NEUROBLASTOMA IMAGING

Imaging for Staging and Therapies

We first attempted and succeeded in imaging neuroblastomas in two children in 1980 because we had demonstrated uptake of ^{14}C-dopamine in human neuroblastomas in 1969 and it was well known that neuroblastomas contained chromaffin granules and frequently secreted dopamine and other precursors of epinephrine (*65*).

Current methods of staging neuroblastoma are imperfect. We have found that MIBG is occasionally more sensitive than are all imaging modalities in differentiating stages I and II of neuroblastoma (*66*).

We and others have also used MIBG to define new dosimetric considerations (*67,68*) and have achieved a 25%–30% incidence of regressions of neuroblastomas with MIBG therapy in patients refractory to conventional therapy.

IMAGING OF OTHER NEUROENDOCRINE TUMORS WITH MIBG

We and others have reported good imaging of carcinoids in the first four of ten patients studied and in three of three nonsecreting paragangliomas, one of five sporadic medullary thyroid cancers, and one of 25 familial medullary thyroid cancers (*69*). Most striking has been the imaging of carcinoid metastases to the peritoneum, liver, and primary bronchial carcinoid. We have imaged two of five chemodectomas, none of four oat cell carcinomas, a choriocarcinoma, an atypical schwannoma, and a Merkel cell skin tumor, but no eyelid cell carcinoma. Most recently, Geatti et al. (*70*) reviewed our use of MIBG in imaging medullary thyroid carcinoma and described their imaging of an insulinoma. We obtained a diagnostic and therapeutic Investigational New Drug (IND) permit for continued diagnostic and therapeutic study of apudoma patients.

IMAGING OF NEUROENDOCRINE TUMORS USING ^{123}I-OCTREOTIDE SOMATOSTATIN RECEPTORS

Pituitary, Acromegaly, and Pituitary Incidentalomas

Growth hormone-secreting adenomas in the pituitary retain both in vitro and in vivo sensitivity to somatostatin, and somatostatin receptors have been identified on the adenoma cells (*71,72*). Somatostatin, however, is not effective therapy, because it has a very short serum half-life (about 2 min) and because the cessation of somatostatin infusion is followed by rebound hypersecretion of growth hormone. It also inhibits insulin secretion.

Recently, a long-acting somatostatin analogue was developed, named octreotide (D-Phe-Cys-Phe-D-Tryp-Lys-Thyr-Cys-Thr [oH]; SMS-201-995, Sandoz). Octreotide is at least 4–5 times more potent than somatostatin in suppressing the secretion of growth hormone, and only about twice as potent in suppressing insulin reaction. It has a serum half-life of about 2 hr after subcutaneous injection. The therapeutic response to octreotide correlates directly with the levels of pituitary tumor somatostatin receptors. A small subgroup of patients do not respond to octreotide, and they may have reduced sensitivity to endogenous somatostatin, possibly due to altered somatostatin-receptor function.

Pituitary-tumor volume shrinks substantially in up to one half the patients who receive octreotide and total tumor disappearance has been reported. Tumor shrinkage appears to be because of a decrease in cell size, with increased intracellular granule storage and perivascular fibrosis. The drug is not cytotoxic, and tumor regrowth occurs after its withdrawal.

Pancreatic and Carcinoid Tumors

Large numbers of high-affinity somatostatin-binding sites have been found on most pancreatic endocrine tumors and carcinoid tumors (*73*). In most patients with such tumors, long-term therapy with octreotide successfully controls clinical symptoms, apparently through the somatostatin receptor-mediated inhibitors of hormone release.

Bakker et al. (*74*) labeled octreotide with ^{123}I, and Krenning et al. (*75*) visualized carcinoid metastases to liver during the intravenous administration of the labeled compound. Lamberts et al. (*76*) recently described the results of this scanning procedure in 42 patients with known endocrine tumors. Primary tumors or metastases, often previously unrecognized, were visualized in 12 of 13 patients with carcinoid tumor and in 7 of 9 patients with pancreatic endocrine tumors. The endocrine symptoms of these patients responded well to therapy with unlabeled octreotide. Among 20 patients with paraganglioma, 8 of

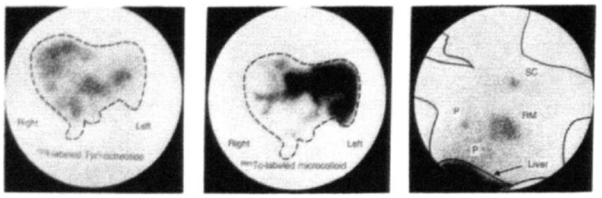

FIGURE 19. Primary tumor and metastases in a patient with metastatic carcinoid disease (*76*). (A) Scintigram of the liver 24 hr after administration of ^{123}I-labeled octreotide. Note the tumor deposits positive for somotostatin receptors, mainly in the right lobe of the liver. (B) Technetium-99m-labeled colloid scan showing least uptake in the areas containing carcinoid metastases. (C) Carcinoid metastases in supraclavicular lymph node (SC), retromediastium (RM), pleura (P) 30 min after administration of labeled octreotide.

whom had more than one tumor, 10 temporal (tympanic or jugular), 9 carotid, and 10 vagal tumors could be visualized. Figure 19 illustrates the primary tumor and metastases in a patient with metastatic carcinoid disease.

Lamberts et al. (*76*) imaged a gastrinoma and metastases but not an insulinoma (*76*). Lamberts et al. concluded (*73*) that ^{123}I-labeled Tyr^3 octreotide scanning technique is a rapid and safe procedure for the visualization of some tumors with somatostatin receptors. A positive scan may predict the ability of octreotide therapy to control symptoms of hormonal hypersecretion.

The obvious next step is to investigate the use of ^{131}I-labeled octreotide for therapy (*76*). The editorial accompanying the article properly emphasized the original use of receptor localization studies for tumors. Receptor localization has been well studied in the brain by other investigators. It is gratifying to see fruitful receptor localization in vivo in human endocrine tumors. However, this radiolabeled compound has not yet received FDA approval and is not commercially available.

REFERENCES

1. Potts JT Jr. Management of asymptomatic hyperparathyroidism. *Clin Rev 9, J Clin Endocrinol Metab* 1990;70:1489–1493.
2. Thompson NW. Localization studies in patients with primary hyperparathyroidism. *Br J Surg* 1988;75:97–98.
3. Thompson NW, Eckhauser FE, Haven JG. The anatomy of primary hyperparathyroidism. *Surgery* 1982;92:814–821.
4. Basarab RM. Editorial: The evolving role of parathyroid scintigraphy. *Clin Nucl Med* 1989;14:58–60.
5. Sisson JC, Beierwaltes WH. Radiocyanocobalamine—(Co57 B12) concentration in the parathyroid glands. *J Nucl Med* 1962;3:160–166.
6. DiGuilio W, Beierwaltes WH. Parathyroid scanning with Selenium 75 labeled methionine. *J Nucl Med* 1964;5:417–427.
7. DiGuilio W, Beierwaltes WH. Parathyroid scanning. In: Wang Y, ed. *Advances in dynamic radioactive scanning*. Springfield, Illinois: Charles C. Thomas, 1968:112–126.
8. Zwas ST, Czerniak P, Boruchowsky S, et al. Preoperative parathyroid localization by superimposed iodine-131 toluidine blue and technetium-99m pertechnetate imaging. *J Nucl Med* 1987;28:298–307.
9. Stark DD, Clark OH, Gooding GAW, Mass AA. High-resolution ultrasonography and computed tomography of thyroid lesions in patients with hyperparathyroidism. *Surgery* 1983;94:863–868.
10. Counsell RE, Ranade VV, Blair RJ, Beierwaltes WH, Weinhold PN. Tumor localizing agents XI radioiodinated cholesterol. *Steroids* 1970;16:317–328.
11. Beierwaltes WH, Lieberman LM, Ansari AN, Nishiyama H. Visualization of the human adrenal in vivo by scintillation scanning. *JAMA* 1971;216:275–277.
12. Lieberman LM, Beierwaltes WH, Conn JW, Ansari AN, Nishiyama H. Diagnosis of adrenal disease by visualization of human adrenal glands with 131I-19-iodocholesterol. *N Engl J Med* 1971;285:1387–1393.
13. Kojima M, Minoru M. Homoallylic rearrangement of 19-iodocholesterol. *JCS Chem Commun* 1975;Jan. 15.
14. Basmadjian GP, Hetzel MR, Ice RD, Beierwaltes WH. Synthesis of a new adrenal cortex scanning agent 6B-I-131-iodomethyl-19-nor cholest-5(10)-en-3β-ol (NP59). *JR Lab Comp* 1975;11:427–434.
15. Sarkar SD, Beierwaltes WH, Ice RD, Basmadjian GP, et al. A new and superior adrenal scanning agent, NP-59. *J Nucl Med* 1975;16:1038–1042.
16. Ryo UY, Beierwaltes WH, Ice RD. Enhancement of uptake with estradiol treatment of radiolabeled irreversible competitive enzyme inhibition in the adrenal cortices and ovaries of rats with endocrine "autonomous" breast carcinoma. *J Nucl Med* 1974;15:187–189.
17. Beierwaltes WH, Wieland DM, Ice RD, et al. Localization of radiolabeled enzyme inhibitors in the adrenal gland. *J Nucl Med* 1976;17:998–1002.
18. Beierwaltes WH, Wieland DM, Mosley ST, Swanson DP, et al. Imaging the adrenal glands with radiolabeled inhibitors of enzyme [Concise Communication]. *J Nucl Med* 1978;19:200–203.
19. Beierwaltes WH, Wieland DM, Swanson DP, Wu T, Mosley ST. Adrenal imaging agents: Rationale, synthesis formulation and metabolism. *Semin Nucl Med* 1979;9:151–155.
20. Gross MD, Shapiro B, Freitas JE, Beierwaltes WH. Experience with 131-I-6-beta-iodomethyl-19-norcholesterol (NP-59) in the functional localization of adrenal cortical disease. Presented at the European Congress of Nuclear Medicine, Helsinki, Finland, August 14–17, 1984.
21. Freitas JE, Gross MD, Swanson DP, Beierwaltes WH. Cost effectiveness of adrenal imaging in Cushing's syndrome [Abstract]. *J Nucl Med* 1979;20:677.
22. Beierwaltes WH, Sturman MF, Ryo UY, Ice RD. Imaging functional nodules of the adrenal glands with 131-I-19-iodocholesterol. *J Nucl Med* 1974;15:246–251.
23. Gross M, Valk T, Freitas JE, Swanson DP, Schteingart DP, Beierwaltes WH. The relationship of adrenal iodomethylnorcholesterol uptake to indices of adrenal cortical function in Cushing's syndrome. *J Clin Endocrinol Metab* 1981;52:1062–1066.
24. Gross MD, Grekin RJ, Brown LE, Marsh DD, Beierwaltes WH. The relationship of adrenal iodocholesterol uptake to adrenal zona glomerulosa function. *J Clin Endocrinol Metab* 1981;52:612–615.
25. Gross MD, Shapiro B, Grekin RJ, Meyers L, Swanson DP, Beierwaltes WH. The relationship of iodomethyl norcholesterol adrenal gland uptake to zona glomerulosa function in primary aldosteronism. *J Clin Endocrinol Metab* 1983;57:477–481.
26. Gross MD, Shapiro B, Freitas JE, Ayers J, Swanson DP, Woodbury MC, Schteingart DE, Beierwaltes WH. The relationship of I-131 6β-iodomethyl-19-norcholesterol (NP59) adrenal cortical uptake to indices of androgen secretion in women with hyperandrogenism. *Clin Nucl Med* 1984;9:264–270.
27. Morita R, Lieberman LM, Beierwaltes WH, Con JW, Ansari AN, Nishiyama H. Percent uptake of 131-I-radioactivity in the adrenal from radioiodinated cholesterol. *J Clin Endocrinol Metab* 1972;37:36–43.
28. Koral KF, Abukhadra H, Tuscan M, Beierwaltes WH. Computing adrenal uptakes with compact fixed-size regions. *Comput Programs Biomed* 1982;15:73–78.
29. Geatti O, Fig L, Shapiro L. Adrenal cortical adenoma causing Cushing's syndrome: Correct localization by function scintigraphy despite nonlocalizing morphological imaging studies. *Clin Nucl Med* 1990;15:168–170.
30. Luten JP, Mahoudeau JA, Bouchard PH, et al. Treatment of Cushing's disease by OPDDD. *N Engl J Med* 1979;300:459–464.
31. Freitas JE, Herwig HR, Cerny JC, Beierwaltes WH. Preoperative localization of adrenal remnants. *Surg Gynecol Obstet* 1977;145:7095–7098.
32. Schteingart DE, Conn JW, Lieberman LN, Beierwaltes WH. Adrenal photoscanning for residual tissue in persistent or recurrent Cushing's syndrome after "total" adrenalectomy. *Arch Intern Med* 1972;140:384–387.
33. Barzilai D, Dickstein G, Kanter T, et al. Complete remission of Cushing's disease by total bilateral adrenalectomy and adrenal autotransplantation. *J Clin Endocrinol Metab* 1980;50:853–855.
34. Prinz RA, Brooks MH, Laurence AM, Paloyan E. Cushing's disease: the role of adrenalectomy and autotransplantation. *Surg Clin North Am* 1979;59:159–165.
35. Shapiro B, Gross MD, Sandler MP. Adrenal scintigraphy revisited: a current status report on radiotracers, clinical utility and correlative imaging.

Freeman LM, Zeissman HS, eds. Presented at the Nuclear Medicine Annual Meeting. New York: Raven Press, 1987:193–232.
36. Conn JW, Beierwaltes WH, Lieberman LM, et al. Primary aldosteronism: Preoperative tumor visualization by scintillation scanning. *J Clin Endocrinol Metab* 1971;33:713–716.
37. Conn JW, Morita R, Cohen EL, Beierwaltes WH, et al. Primary Aldosteronism Photoscanning of tumors after administration of 131-I-19-iodocholesterol. *Arch Intern Med* 1972;129:417–425.
38. Seabold VE, Cohen EL, Beierwaltes WH, et al. Adrenal imaging with 131-I-19-iodocholesterol in the diagnostic evaluation of patients with aldosteronism. *J Clin Endocrinol Metab* 1976;42:41–51.
39. Miles JM, Wahner HW, Corpester PC, et al. Adrenal scintiscanning with NP-59: A new radioiodinated cholesterol agent. *Mayo Clin Proc* 1979;54:321–323.
40. Gunnels JC, McGriffin WZ, Robinson RR, et al. Hypertension, adrenal abnormalities and alterations in plasma renin activity. *Ann Intern Med* 1970;73:901–910.
41. Rifai A, Beierwaltes WH, Freitas JE, Grekin R. Adrenal scintigraphy in low renin essential hypertension. *Clin Nucl Med* 1978;3:282–286.
42. Gross MD, Freitas JE, Swanson DP, Bradley T, Beierwaltes WH. The normal dexamethasone suppression adrenal scintiscan. *J Nucl Med* 1979;20:1131–1135.
43. Gross DD, Shapiro B, Grekin RV, Freitas JE, Glaser G, Beierwaltes WH, Thompson NW. Scintigraphic localization of adrenal tumors in primary aldosteronism. *Am J Med* 1984;77:839–844.
44. Nomurs K, Kizako H, Masako M, et al. Iodomethynorcholesterol uptake in an aldosteronoma shown by dexamethasone suppression scintigraphy: Relationship to adenoma size and functional activity. *J Clin Endocrinol Metab* 1990;71:825–830.
45. Freitas JE, Beierwaltes WH, Nishiyama RH. Adrenal hyperandrogenism: Detection by adrenal scintigraphy. *J Endocrinol Invest* 1978;1:59–64.
46. Ehrmann DA, Rosenfield RL. Clinical review 10. Endocrinologic approach to the patient with hirsutism. *J Clin Endocrinol Metab* 1990;71:1–4.
47. Gross MD, Wortsman J, Shapiro B, et al. Scintigraphic evidence of adrenal cortical dysfunction in the polycystic ovarian syndrome. *J Clin Endocrinol Metab* 1985;62:197–201.
48. Schultz CL, Haaga JR, Fletcher BD, et al. Magnetic resonance imaging of the adrenal glands: A comparison with CT. *AJR* 1984;143:1235–1240.
49. Carpenter PC, Wahner HW, Salassa RM, Duick DS. Demonstration of steroid producing gonadal tumors by external scanning with the use of NP-59. *Mayo Clin Proc* 1979;54:332–335.
50. Ripley DS, Gross MD, Shapiro B, et al. Scintigraphic localization of androgen secreting neoplasm. *Eur J Nucl Med* 1985;11:A27.
51. Gross MD, Shapiro B, Bouffard AV, et al. Distinguishing benign from malignant euadrenal masses. *Ann Intern Med* 1988;109:613–618.
52. Beierwaltes WH. History of development of imaging of chromaffin granule containing tumors. In McEwan AJB, ed. *Clinical use of MIBG for diagnosis and therapy*. Boca Raton, Florida: CRC Press, 1990.
53. Beierwaltes WH. Clinical applications of 131-I-labeled Metaiodobenzylquanidrine. James L. Quinn III Memorial Essay. In: Hoffer PB, ed. *1987 Yearbook of nuclear medicine*. Chicago: Yearbook Medical Publishers, 1987:17–34.
54. 131-I Metaiodobenzylguanidine Imaging Agent and Method of Use. Patent #4,584,187, April 22, 1986.
55. Carmichael SW, Winkler H. The adrenal chromaffin cell. *Sci Am* 1985;253:40–49.
56. Valk TW, Frager MS, Gross MD, et al. Spectrum of pheochromocytoma in multiple endocrine neoplasia: a scintigraphic portrayal using 131-metaiodobenzylquanidine. *Ann Intern Med* 1981;94:762–767.
57. Beierwaltes WH, Sisson JC, Shapiro B, et al. Malignant potential of pheochromocytoma (P): implications for follow-up. *Clin Res* 1986;34:713A.
58. Manger WM, Gifford RW Jr. Hypertension secondary to pheochromocytoma. *Bull NY Acad Med* 1982;58:139–158.
59. Shapiro B, Copp JE, Sisson JC, et al. ^{131}I-meta-iodobenzylguanidine for the locating of suspected pheochromocytoma. Experience in 400 cases. *J Nucl Med* 1985;26:576–585.
60. Freier DT, Harrison TS. Rigorous biochemical criteria for the diagnosis of pheochromocytoma. *J Surg Res* 1973;14:117–180.
61. Freier DT, Eckhauser FE, Harrison TS. Pheochromocytoma: a persistently problematic and still potentially lethal disease. *Arch Surg* 1980;115:388–391.
62. Sisson JC, Shapiro B, Beierwaltes WH, et al. Treatment of malignant pheochromocytoma with a new radiopharmaceutical. *Trans Assoc Am Physicians* 1983;96:209–217.
63. Sisson JC, Shapiro B, Beierwaltes WH, et al. Radiopharmaceutical treatment of malignant pheochromocytoma. *J Nucl Med* 1984;25:197–206.
64. Sisson J, Shapiro B, Glowniak J, et al. I-131-metaiodobenzylguanidine treatment of malignant pheochromocytomas [Abstract]. *J Nucl Med* 1984;25:72.
65. Lieberman LM, Beierwaltes WH, Varma VM, et al. Labeled dopamine concentration in human adrenal medulla and in neuroblastoma. *J Nucl Med* 1969;10:93–97.
66. Geatti O, Shapiro B, Sisson JC, et al. I-131-metaiodobenzylguanidine (131-I-MIBG) scintigraphy for the location of neuroblastoma: preliminary experience in 10 cases. *J Nucl Med* 1985;26:736–742.
67. Beierwaltes WH. Uptake in basic research and clinical experience with MIBG. *Med Pediatr Oncol* 1987;15:113–169.
68. Beierwaltes WH. Treatment of neuroblastoma with I-131-MIBG. Dosimetric problems and perspectives. *Med Pediatr Oncol* 1987;15:187–191.
69. Von Moll L, McEwan AJ, Shapiro B, Sisson JC, Gross MD, Beierwaltes WH, Thompson NW. Iodine-131 MIBG scintigraphy of neuroendocrine tumors other than pheochromacytomas and neuroblastomas. *J Nucl Med* 1987;28:979–988.
70. Geatti O, Shapiro B, Barillari B. Scintigraphic depiction of an insulinoma by I-131-metaiodobenzyl-quanidine. *Clin Nucl Med* 1989;14:903–905.
71. Melmud S. Acromegaly, medical progress [Review Articles]. *N Engl J Med* 1990;322:966–975.
72. Mayse E, LeDafniet M, Egelbaum J, et al. Somatostatin receptors in human growth hormone and prolactin secreting pituitary adenomas. *J Clin Endocrinol Metab* 1985;61:98–103.
73. Lamberts WJ, Bakker WH, Reubi JC, Krenning EP. Somatostatin receptor imaging in the localization of endocrine tumors. *N Engl J Med* 1990;323:1246–1249.
74. Bakker WH, Krenning EA, Breeman WA, et al. Receptor scintigraphy with a radioiodinated somatostatin analogue: Radiolabeling, purification, biological activity and in vivo application in animals. *J Nucl Med* 1990;31:1501–1509.
75. Krenning EP, Bakker WH, Breeman WAD, et al. Localization of endocrine related tumors with radioiodinated analogue of somatostatin. *Lancet* 1989;1:242–244.
76. Lamberts WJ, Hofland LJ, van Koetsveld PM, et al. Parallel in vivo and in vitro detection of functional somatostatin receptors in human endocrine pancreatic tumors; consequences with regard to diagnosis, localization, and therapy. *J Clin Endocrinol Metab* 1990;71:566–574.
77. Gross MD, Shapiro B, Thrall JH, Freitas JE, Beierwaltes WH. The scintigraphic imaging of endocrine organs. *Endocr Rev* 1984;5:221–281.
78. Gross MD, Volk JT, Swanson DP, et al. The role of pharmacologic manipulation in adrenocortical scintigraphs. *Semin Nucl Med* 1981;9:128–148.
79. Sisson JC, Frager RS, Volk TW, Gross MD, Swanson DP, Wieland DM, Tobes MC, Beierwaltes WH, Thompson NW. Scintigraphic localization of pheochromocytoma. *N Engl J Med* 1981;305:12–17.
80. Beierwaltes WH, Sisson JC, Shapiro B: Diagnosis of adrenal tumors with radionuclide imaging. In: Foâ PP, Cohen MP, eds. *Special topics in endocrinologic metabolism*. New York: Alan R. Liss, Inc., 1984:1–54.